The Control Concept for Upper Limb Exoskeleton

Bianca Lento
University of Nantes
Yannick Aoustin (Yannick.Aoustin@univ-nantes.fr)
University of Nantes
Teresa Zielinska
Warsaw University of Technology

Research Article

Keywords: Limb Exoskeleton, EMG, Robotic, fuzzy logic

Posted Date: December 1st, 2021

DOI: https://doi.org/10.21203/rs.3.rs-1101439/v1

The Control Concept for Upper Limb Exoskeleton

Bianca Lento[1,+], Yannick Aoustin[1,*,+], and Teresa Zielinska[2,+]

[1]University of Nantes, LS2N UMR CNRS 6004 1, rue de la Noë BP 92101 44321 NANTES Cedex 3
[2]Warsaw University of Technology, Faculty of Power and Aeronautical Engineering,Nowowiejska 24, 00-665 Warsaw
[*]corresponding author: Yannick.Aoustin@univ-nantes.fr
[+]these authors contributed equally to this work

ABSTRACT

Robotic exoskeletons inspired by the animal's external covering are wearable systems that enhance human power, motor skills, or support the movement. The main difficulty, apart from the mechanical structure design, is the development of an exoskeleton control system, as it should recognize the movement intended by the user and assist in its execution.
This work is devoted to the exoskeleton of the upper limbs that supports movement. The method of controlling the exoskeleton by means of electromyograms (EMG) was presented. EMG is a technique for recording and assessing the electrical activity produced by skeletal muscles. The main advantage of EMG based control is the ability to forecast intended motion, even if the user is unable to generate it. This work aims to define strategies for controlling the exoskeleton of the upper limb in children suffering from neuromuscular diseases. Such diseases gradually reduce the mobility of the lower and upper limbs. These children are wheelchair bound, so it was assumed that the upper limb exoskeleton could be attached to a wheelchair.
EMG signals are recorded, amplified and filtered. An artificial neural network using fuzzy logic to process EMG was used. This network predicts movement trajectories. Using this forecast and taking into account the feedback information, the control system generates the appropriate drive torques.

1 Introduction

The exoskeleton is an integrated mechanical device that can be worn and attached to the limbs to increase the handling capacities of the human or to compensate for his muscular weakness[1,2]. The range of applications of robotics exoskeleton is wide and in continuous expansion. Many are the fields in which using these wearable devices has significant benefits: for example, in the manufacturing sector exoskeletons are empowering the workforce increasing production efficiency and reducing human injuries,[3,4], or[5]. However, the most challenging applications of these assistance devices are related to the medical field,[6,7,8], or[9]. As a matter of fact, exoskeletons are designed to help patients with rehabilitation to restore motion skills and also improve the level of physical activity after years of injury. Moreover, these robots represent a good solution for patients affected by neuromuscular diseases, such as neuropathy and myopathy, providing essential support during the motion. Thus, through the assistance of these wearable robots, these patients could be more independent and autonomous in their life, executing daily tasks such as grasping an objects, eating, or walking. Van Dijsseldonl *et al* in[10] presented a study that provides the amount, purpose, and location of exoskeletons use by persons with spinal cord injury (SCI). The patients reported satisfaction with the exoskeleton for exercising and social interactions at home and within the community, but reported limitations as an assistive device during normal daily life. There is still much progress to be made in the development of exoskeletons.

Due to the complexity of a human limbs motion dynamics, the development of exoskeletons control methods is not a trivial task. According to[11], the exoskeleton control systems can be basically classified into two categories:

- physical parameters-based control systems, that can be divided into position controllers[12] and force/torque controllers[13]
- model-based control systems, that can be divided into dynamic model-based controllers[14] and muscle model-based controllers

Muscle model-based controllers predict the muscle forces as a function of muscle neural activities and joint kinematics by using either the Hill muscle model[15] or directly computing the torques from the EMG signals[16,17].

This work describes the implementation of an EMG-based control system dedicated for an upper limb exoskeleton for children suffering from neuromuscular diseases.

This paper is structured in the following way: the present section introduces the work and its outline, section 2 addresses the problem statement, section 3 analyzes the biomechanics of the upper limb, section 4 presents the used dataset, section 5 describes the proposed control system concept, section 6 illustrates the obtained results and analyzes the error in estimating both angular trajectories and torques. Section 7 summarizes the objective achieved within this project and illustrates possible future works.

2 Statement of the problem

Among many potential options, muscle interfacing seems to be one of the most suitable solutions for controlling exoskeletons. Even if muscular recordings are peripheral measurements (delivered by surface sensors) and not obtained directly from the nerve cells, they contain neural information on the executed tasks. Consequently, the *EMG* signal is strictly associated with the neural one.

Thus, from these signals, it is possible to estimate both the human motion and the force exerted by the user on the environment. The main benefit is that the user does not need to supervise the joint control because the controller directly attempts the intended motion.

Another advantage of using *EMG*-based control is represented by the surface *EMG* sensors as they are safe, non-invasive, have a relatively easy application and allow gathering the signal at the surface of the skin.

The major drawback is that the features of the *EMG* signal can be altered significantly by a lot of factors including changes of the electrode position or in the impedance of the electrode, muscle fatigue, cross-talk among adjacent muscles and even the skin thickness.

This work supports the design of an upper limb exoskeleton for children suffering from neuromuscular diseases. Generally, these children are already not able to walk, which is limiting their motion to the use of the wheelchair, so an upper limb exoskeleton is proposed as a solution to preserve the motion independence of the upper part of their body. Therefore, the use of this wearable robot represents a motivating way to improve their motion abilities and therefore their life.

An artificial neural network (*NN*) applying fuzzy logic to the pre-processed *EMG* signals was implemented. The Fuzzy Logic Toolbox from Matlab® was used to predict the movement. Basis on this forecast and taking into account the feedback the concept was tested. For this purpose the inverse dynamic model of the limb system was implemented in Matlab. Through the Lagrangian formulation and using as an input the difference between the predicted joint angles and the actual joint angles measured by the motion capture system, the torques needed for actuating the exoskeleton were obtained.

3 Biomechanics of the upper limb

The upper limb is composed of three main parts: the shoulder, the elbow, and the wrist with the hand, Fig. 1. However, considering the features of this project, the analysis will be focused only on the first two parts. As shown in the following figure, each part is composed of bones, muscles, and joints.

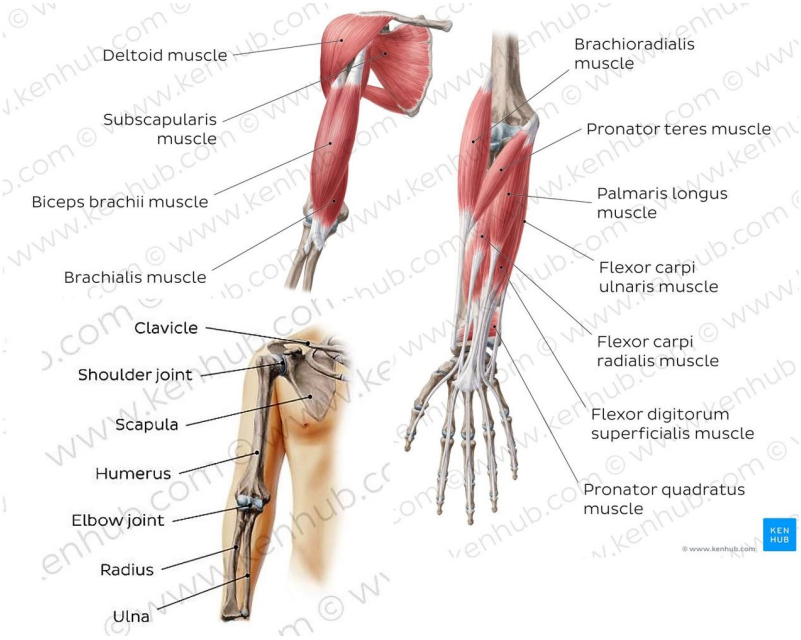

Figure 1. Upper limb,[18].

The shoulder is a complex joint able to perform omnidirectional movements, while the elbow is a hinge joint as it bends and straightens like a hinge. Another movement also occurs where the radius meets the humerus, which allows turning the hand palm up and down.

Considering the complexity of the shoulder joint, it was chosen to base this work on a simplified model of the upper limb

which consists of two parts - the upper arm and the forearm with two joints - the shoulder and the elbow, - one degree of freedom (*DoF*) each, Fig 2.

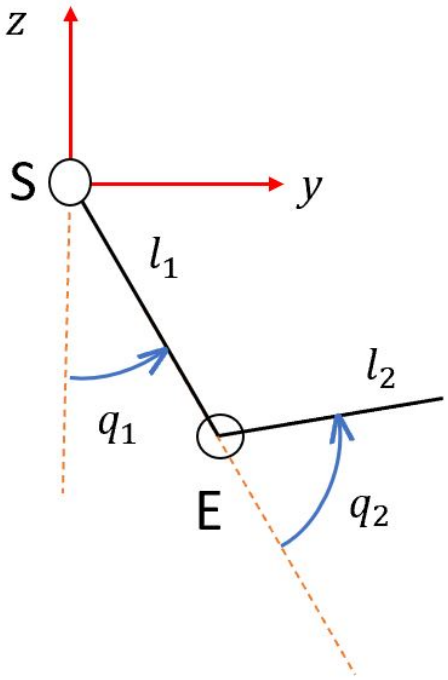

Figure 2. Simplified kinematic model.

The body reference frame is attached to the centre of the shoulder (S). Parameters l_1 and l_2 are the lengths of the upper arm and the forearm respectively. The joint variables, q_1 and q_2, represent the rotation of the shoulder and the elbow around the x-axis, meaning the flexion/extension motion. Therefore, these simplifications lead to describing the dynamic model of the upper limb as follows.

$$\mathbf{D}(\mathbf{q})\ddot{\mathbf{q}} + \mathbf{C}(\mathbf{q}, \dot{\mathbf{q}}) = \mathbf{D}_\Gamma \Gamma \tag{1}$$

Here $\mathbf{q} = (q_1, q_2)^\top$, $\mathbf{D}(\mathbf{q})(2 \times 2)$ is a symmetric positive definite inertia matrix, $\mathbf{C}(\mathbf{q}, \dot{\mathbf{q}})(2 \times 1)$ is a vector, which groups the centrifugal, Coriolis, and gravity forces. Vector $\Gamma(2 \times 1)$ groups the applied joint torques applied in the shoulder and elbow. $\mathbf{D}_\Gamma(2 \times 2)$ is a matrix composed of the 0 and ± 1 given by the principle of virtual works[19].

Flexion and extension are the joint actions that move the limb in the sagittal plane. The main muscles involved during the shoulder flexion are the pectoralis major and the anterior deltoid; during the extension, the latissimus dorsi, and the posterior deltoid[20]. The elbow flexion is achieved by triceps brachii and anconeus while the extension by brachialis, biceps brachii, brachioradialis[21].

4 Dataset

The dataset used in this work was provided be the Warsaw Children Memorial Hospital and consists of twelve trials in which a healthy male adult subject performs the flexion/extension motion of the elbow holding different loads in the hand (0, 1, 2, and 5 kG). The trials are arranged in three groups of four trials each, depending on the position of the subject. In the first group, the subject stands upon one force platform during the recording of the motion. In the second group, he stands upon two platforms, while in the third group, he is seated. The dataset includes the *EMG* data recorded from 16 channels, attached to the main muscles of the upper limb, the positions and the angles of the whole body acquired by using capture motion device, the moments and the forces of several parts of the body. Moreover, the provided *EMG* data were already processed: the signals were amplified to a range of $0 - 5$V and filtered to reduce the noise.

In our research, two features were extracted from the *EMG* signal recorded from channels number 10 and 14 and used as inputs for the fuzzy neural network. It was chosen to use these channels as their electrodes are above the main muscle group that contracts more intensively during the performance of the designed movements. The data were recorded using VICON system

with the dedicated software. Besides of the research purposes, the system is used by hospital for diagnosing the children's neural diseases, and for testing the rehabilitation and medication processes.

The selected features were the root mean square (*RMS*) and the maximum fractal length (*MFL*), obtained using a software package, developed with Matlab by T. Jingwei *et al*[22]. The feature *RMS* characterizes the magnitude of the signal: it represents the effective value of the electrical signal and it gives a measure of the signal power. It is computed using the equation below:

$$RMS = \sqrt{\frac{1}{N}\sum_{i=1}^{N} x_i^2} \tag{2}$$

in which x_i is the signal value at i-th sampling and N is the number of samples in a data segment.

The feature *MFL* represents the density of motor unit action potential, in other words, the muscle contraction strength[23], it is computed by the following formula:

$$MFL = \log_{10}\left(\sqrt{\sum_{i=1}^{N-1}(x(i+1)-x(i))^2}\right) \tag{3}$$

in which N is the signal length, while x is the signal. As shown in the literature, it is very similar to the waveform length on a logarithmic scale, thus it is less sensitive to the noise.

5 The control system design

The block diagram of the proposed control concept is given in Fig. 3.

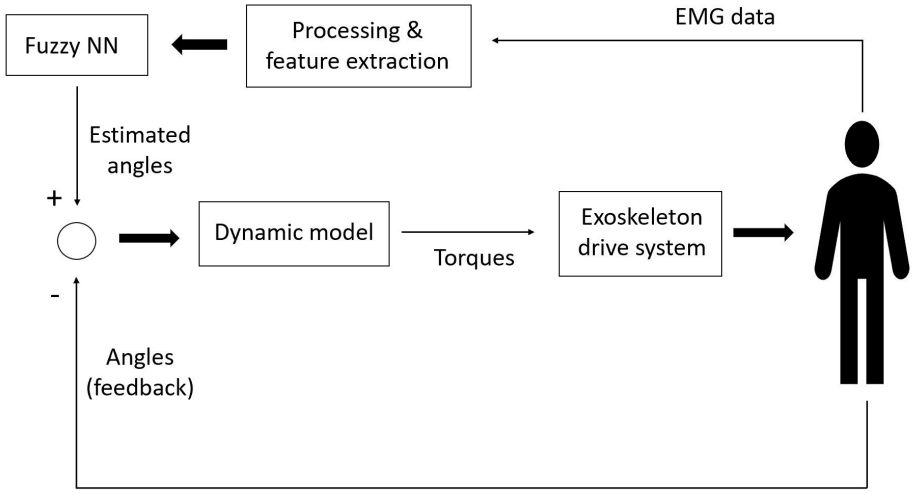

Figure 3. Control system design.

The *EMG* signals are acquired from the subject to retrieve information about the muscle activity. Since the measurements are easily affected by disturbances, the signals are filtered and processed. Two features, the *RMS* and the *MFL*, were extracted from the signals and used as inputs for the fuzzy *NN* to predict the angular trajectories. The angles are delivered by the fuzzy *NN*. The result is compared with the actual angles and based on this difference, the driving torques are determined. The torques should be applied to the exoskeleton drive system. In our case the exoskeleton is still in the design stage, therefore we used the detailed model of the upper limb available in the *OpenSim* instead.

Fuzzy *NN*

An adaptive network using fuzzy logic was implemented in such way that, based on the processed *EMG* signals, it was able to estimate the intended angular position, Fig 4. The inputs are the *RMS* and the *MFL* extracted from the processed *EMG* signal. As stated before, the first one characterizes the amplitude of the *EMG* signal, while the second one is proportional to the

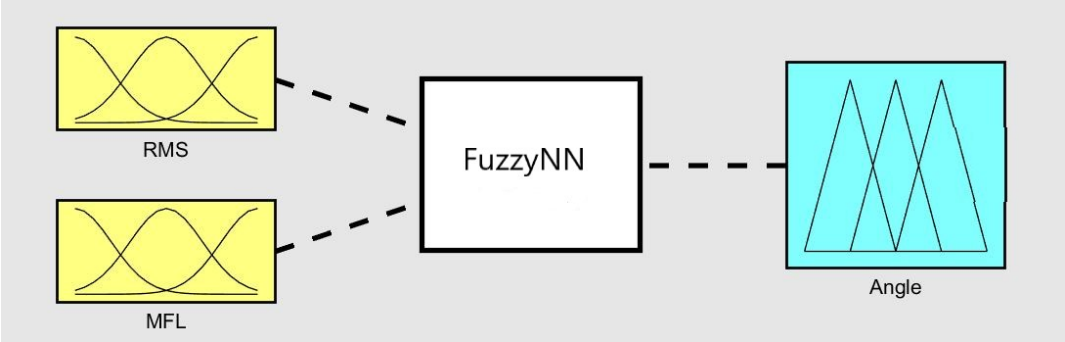

Figure 4. Fuzzy *NN*.

strength of muscle contraction.

The fuzzy *NN* is a hybrid system of fuzzy logic and *NN* technique. In fact, while fuzzy logic deals with the imprecision and the uncertainty of the system, the *NN* gives it a sense of adaptability. The model scheme of a fuzzy *NN* is shown Fig. 5. The fuzzy *NN* is governed with the following IF-THEN rules[24]:

- If x is A_1 and y is B_1, then f = C_1;
- If x is A_2 and y is B_2, then f = C_2;

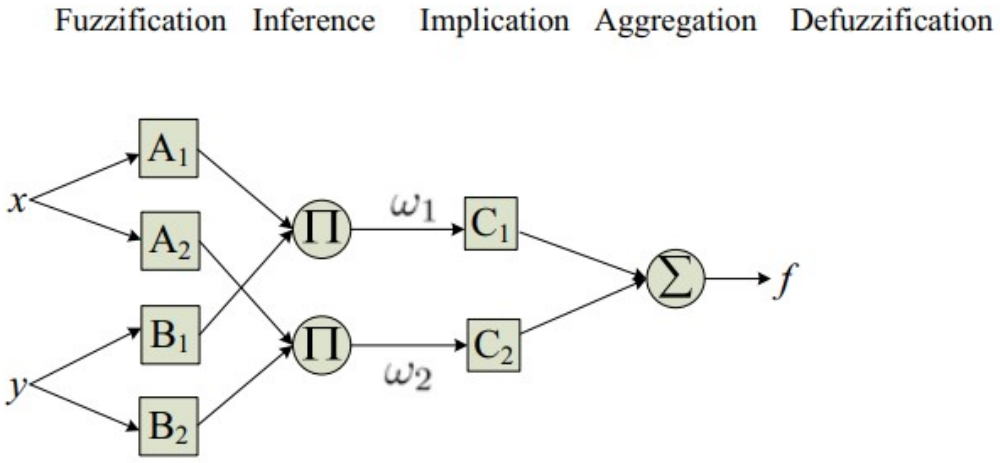

Figure 5. Fuzzy *NN* architecture.

The IF-THEN rules define the state of the output depending on the state of the inputs, following such principle: IF the input variable is in a certain state, THEN the output will have that specific state. Available in Matlab Mandani type[25] of fuzzy *NN* was applied.

The architecture of the fuzzy *NN* consists of five layers. The fuzzification layer takes the input values and determines the membership functions belonging to them. The inference layer generates the firing strengths for the rules with product method. In the implication and the aggregation layers, the computed firing strengths are normalized and aggregated respectively. The defuzzification layer returns the output.

For the elbow, the input space was assigned to three fuzzy sets: low, medium and high, Fig. 6. Each set represents the intensity of the muscle activation: when the input belongs to the low fuzzy set, the muscle is resting, when it belongs to the medium, the muscle is powering the motion; while when it belongs to the high, the contraction of the muscle is very intense. To increase the accuracy of the results in both inputs, the medium set was divided into two subsets and as the *MFL* ranges from 0 to 2, the same logic was applied to the high set.

The choice of Gaussian function increases the sensitivity of the system and allows obtaining smoother results. The functions

present almost the same width, which is found by trials and errors.

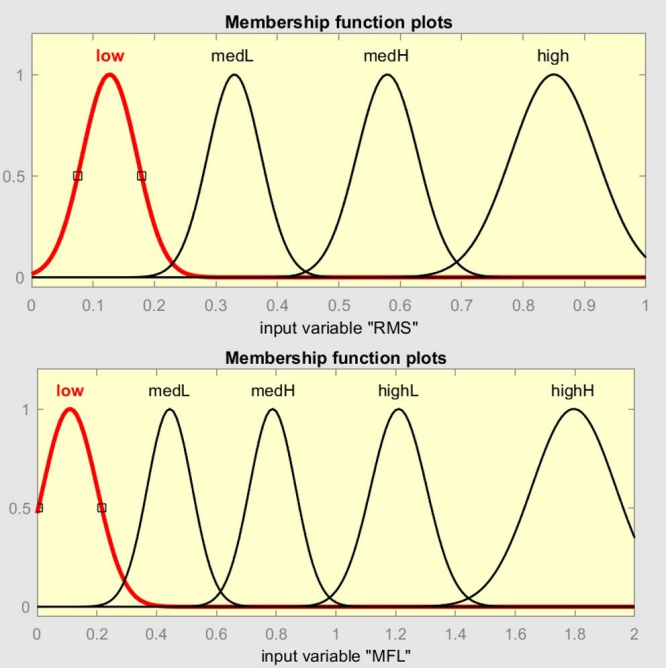

Figure 6. Membership functions inputs - elbow.

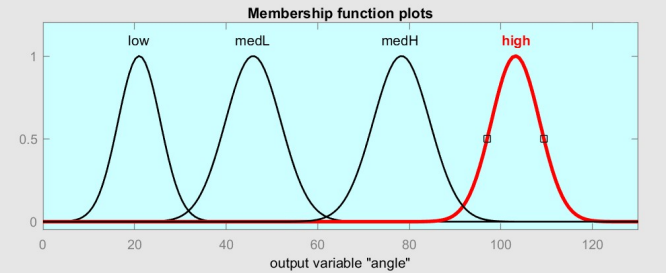

Figure 7. Membership functions output - elbow.

The same logic was applied for the output, Fig. 7. The relationships between the inputs and the output are defined through the following IF-THEN rules:

1. If (*RMS* is low) and (*MFL* is low) then (angle is low)
2. If (*RMS* is medL) and (*MFL* is medL) then (angle is medL)
3. If (*RMS* is medL) and (*MFL* is low) then (angle is medL)
4. If (*RMS* is medH) and (*MFL* is medL) then (angle is medH)
5. If (*RMS* is medH) and (*MFL* is medH) then (angle is medH)
6. If (*RMS* is medH) and (*MFL* is highL) then (angle is high)
7. If (*RMS* is high) and (*MFL* is highL) then (angle is high)

The fuzzy *NN* of the shoulder was more complicated to implement as the motion performed in the given dataset is very limited. The logic behind the implementation of the membership functions is the same as for the elbow, Figs 8, 9. For the *RMS*, it is noticed that merging the medium and the high sets into a unique one improves the accuracy of the results.
To characterize the output status depending on the inputs, the following IF-THEN rules are formulated:

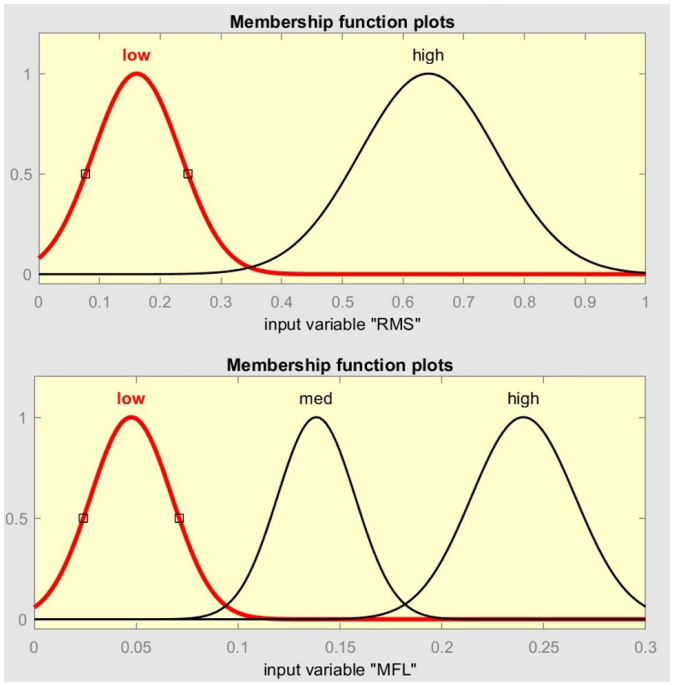

Figure 8. Membership functions inputs - shoulder.

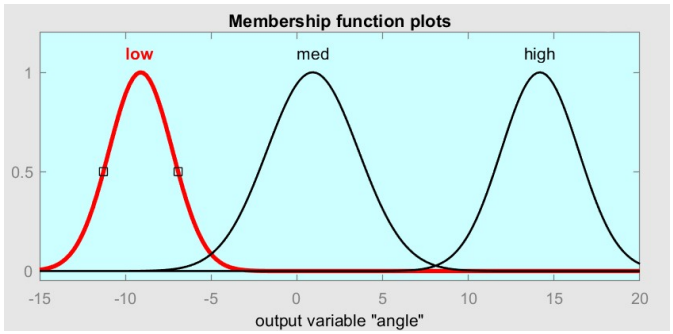

Figure 9. Membership functions output - shoulder.

1. If (*RMS* is low) and (*MFL* is low) then (angle is low)
2. If (*RMS* is low) and (*MFL* is med) then (angle is low)
3. If (*RMS* is low) and (*MFL* is high) then (angle is med)
4. If (*RMS* is high) and (*MFL* is low) then (angle is med)
5. If (*RMS* is high) and (*MFL* is med) then (angle is high)
6. If (*RMS* is high) and (*MFL* is high) then (angle is high)

6 Results

To test the accuracy of the angles prediction, the obtained angles were compared with the adequate angles of a human upper limb. The computed and real torques were compared as well. Obtained results are discussed below.

The *EMG* signal is a biological signal which directly reflects human muscle activities generated when the muscles contract. Thus, it is the reflection of the user's motion intention that allows estimating the movement before it is effectively performed.

For both shoulder and elbow, Figs. 10 and 11 shows the angular trajectories obtained from the fuzzy *NN* and the actual angular trajectories, which were delivered by the VICON motion capture system at 100 Hz. The angular trajectories from the

fuzzy *NN* are advanced in time towards the actual angles, meaning that the proposed control method is predictive. Therefore, for testing the control system, it was necessary to evaluate the time shift of the fuzzy *NN* outputs to coincide with the actual movement.

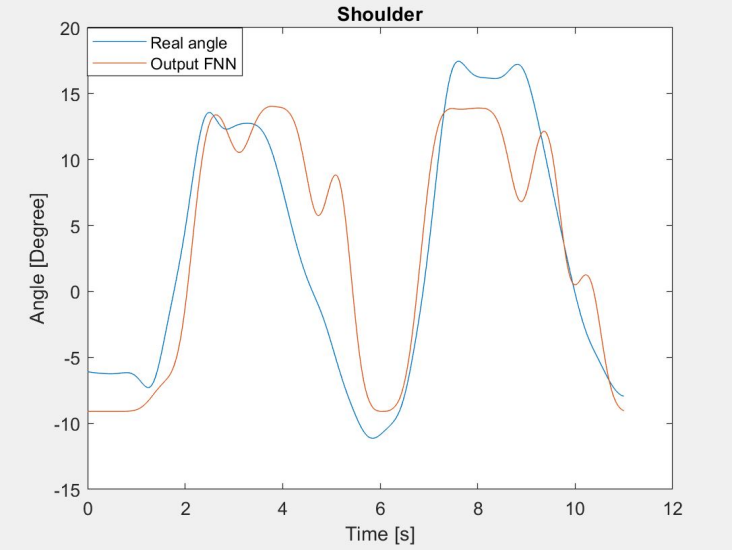

Figure 10. Shifted Fuzzy *NN* results - shoulder.

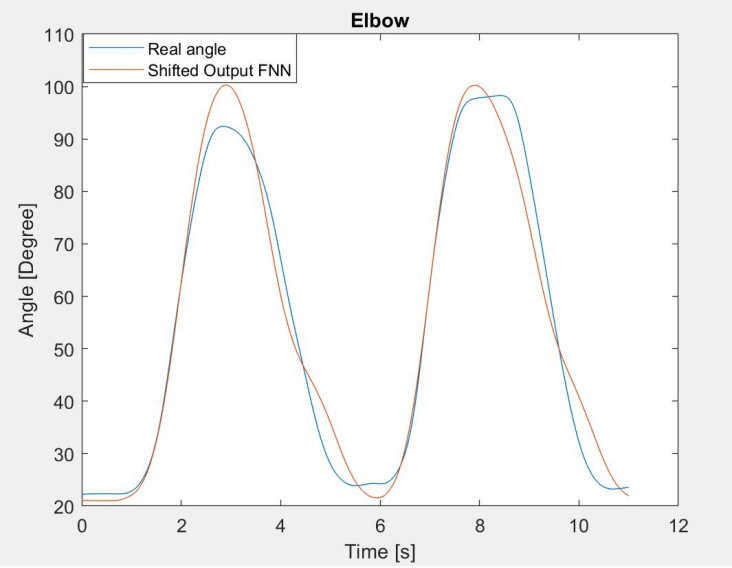

Figure 11. Shifted Fuzzy *NN* results - elbow.

The motion estimation error was expressed as the difference between the shifted output of the fuzzy *NN* and the actual angle delivered by the capture motion system, Fig. 12. In the shoulder, it is in the range $[-5,5]^\circ$ during almost all the time. However, in the time $4-6$s, the error is bigger, reaching its peak of nearly 15°. In the elbow, the error is near to zero for the first two seconds and in the time $6-8$s, which is the resting and the flexion, while during the extension, it varies from -10 to 10°.

Analyzing these results, the Bland & Altman method[26] was applied to compare the two angular trajectories and quantify the compatibility of the angles from the fuzzy *NN* and the actual angular trajectories (delivered by the motion capture system). Firstly the comparison was made for the shoulder (Fig. 13). For each sampling time the difference between the fuzzy *NN* output and the actual angular trajectories is plotted against the average. It was detected that 93% of the differences between the results from the fuzzy *NN* and the actual angular trajectories lie between the limits of agreement, represented by red dotted horizontal lines. It means that there is a certain degree of similarity between the two methods, however the level of agreement is

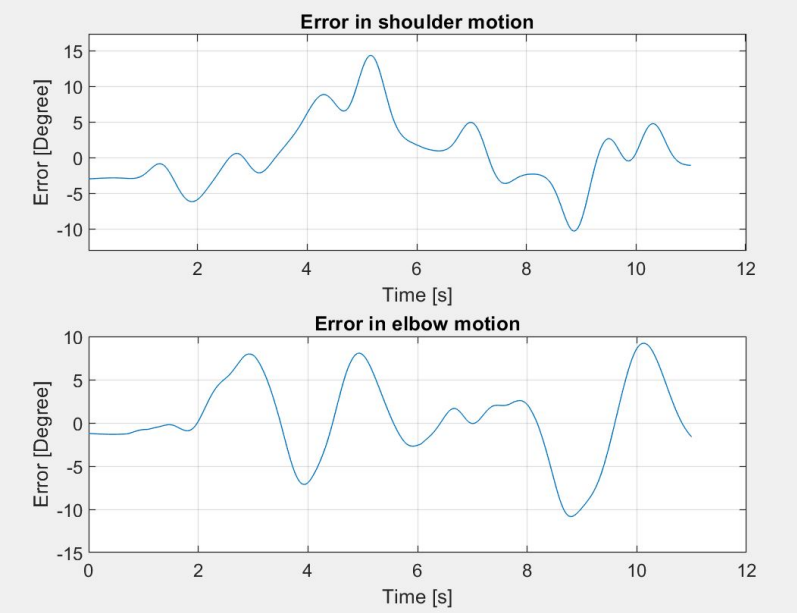

Figure 12. Difference between the output of the fuzzy *NN* and the recorded motions for the shoulder and elbow.

a bit lower than expected.

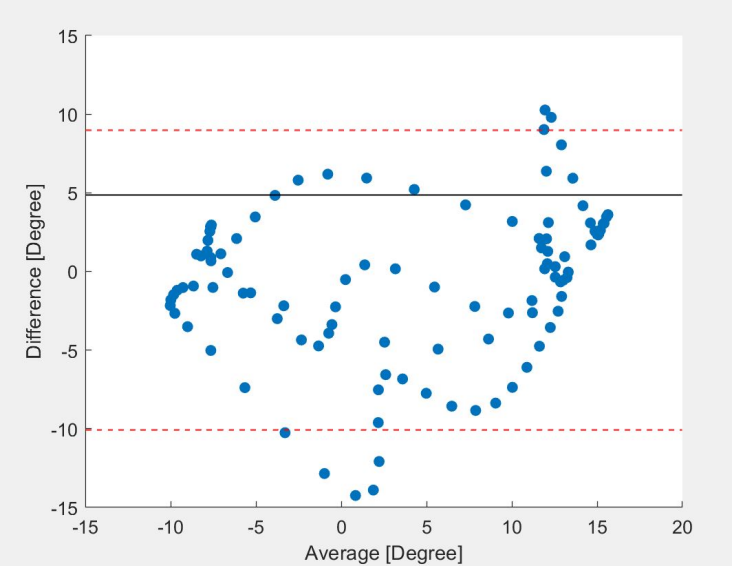

Figure 13. Bland-Altman method applied for the shoulder motions.

For the elbow, 95% of the difference lies between the limits of agreement, which proves that there is strong correlation and agreement between the results delivered by the the fuzzy *NN* and the real angular trajectories , Fig.14.

As the proposed control system is predictive for both shoulder and elbow, it is expected that torques, which are computed using the inverse dynamic model (1), are earlier in time towards the actual torques provided by the dataset. For both, the shoulder and elbow the comparison of torque trajectories is shown in Figs. 15 and 16.

The computed torques are slightly shifted in time towards the actual trajectories, some small discrepancies in shape are mainly due to the use of simplified planar two-link model (1). The most significant difference is in the minima, as the computed torques don't reach the same values as the actual ones. Moreover, in the shoulder plot, in the time interval $4-6$s, a bit bigger difference between the two trajectories is observed, such phenomenon is caused by the local inaccuracy in the shoulder angle

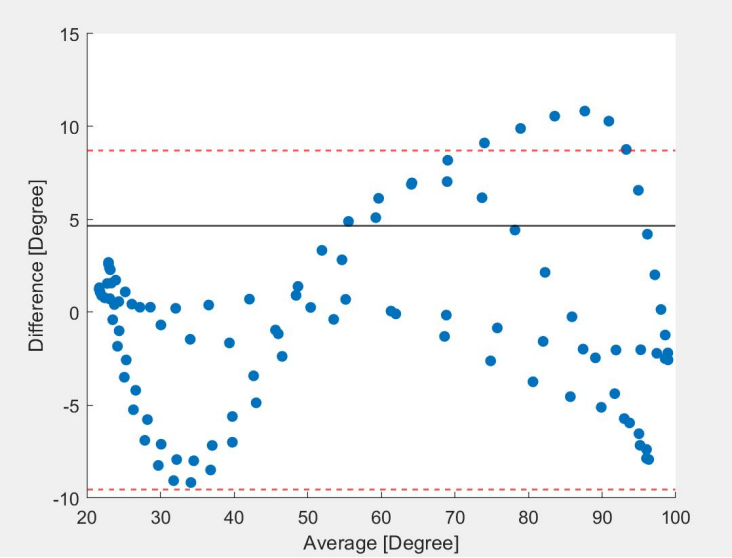

Figure 14. Bland-Altman method applied for the elbow motions.

estimation by the fuzzy *NN*. The elbow torque estimation error is smaller than that of the shoulder, and is ranging $[-0.5; 0.5]$ Nm.

6.1 Final validation using *OpenSim*

To validate the proposed control strategy, it was chosen to simulate the motion using *OpenSim*[27], which is a software system dedicated for building and analyzing computer models of the musculoskeletal system and for dynamic simulation of the movement.

The movement analyzed in this work is the flexion/extension of the shoulder and the elbow joints, therefore it was possible to use the *OpenSim* model called "Arm26", which is a right upper extremity model with two *DoF* (flexion/extension of the shoulder and the elbow) and with three main muscle groups (biceps, triceps, and brachialis).

After scaling the physical parameters of the model according to the subject characteristic, the motion was simulated using the angular trajectories delivered by the fuzzy *NN*. The torques were calculated using the simplified dynamic model developed for controller. Next, for the real motion trajectories recorded by the motion capture system the motion was simulated using *OpenSim* and *Arm26* and the corresponding torques were obtained.

Both torque trajectories obtained using simplified model presented some noise and were not as smooth as the ones delivered by the *OpenSim*. This difference is a consequence of the numerical schemes used for calculating the velocities and accelerations. *OpenSim* has its efficient procedures for it, in which the data is filtered with a lowpass filter with a cut-off frequency of 6Hz. In this work, the velocities and the accelerations were computed using linear approximation and then smoothed with a moving average.

Without considering the discrepancies due to numerical schemes, the torques delivered by the control system represented in Fig. 3, follow the same path as the torques computed by the *OpenSim* (Fig. 17 and Fig. 18). In some segments, especially during the flexion, the two trajectories overlap perfectly while in other parts, there are small differences. For the elbow, the most evident difference is that the torque computed by *OpenSim* reaches peaks almost 0.5Nm bigger than the torque delivered by the control system. Moreover, there is a small time difference in both; flexion and extension motion performances.

7 Conclusion

In this paper, an *EMG*-based control system was developed as a part of the design of an upper limb exoskeleton to assist the flexion/extension motion of the shoulder and the elbow.

The proposed control system was able to correctly estimate the angular trajectories and the torques needed for actuating the exoskeleton, especially for the elbow. However, due to the limited motion records, the difference between the shoulder torques

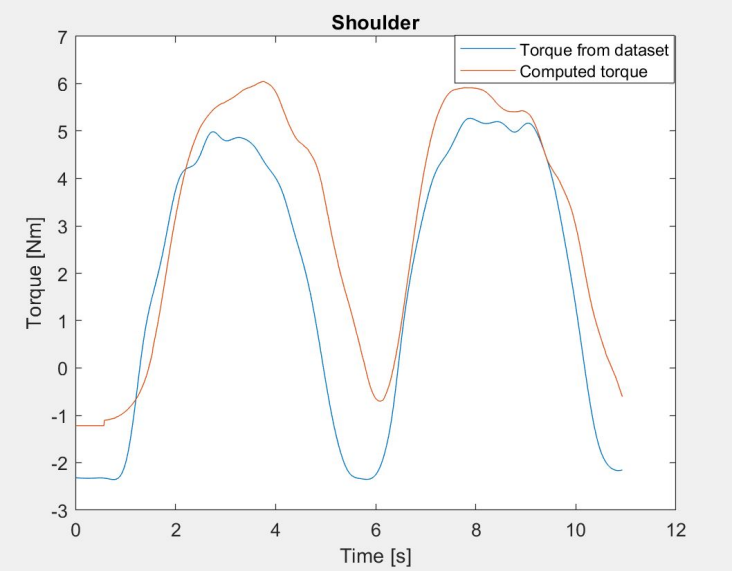

Figure 15. Shoulder: comparison of the computed torques and the torques provided by the dataset.

obtained from the control system and that one given in the dataset is little more significant than that for the elbow.

Future developments should include:

- the improvement of the results by optimizing the parameters of the membership functions of the fuzzy *NN*,
- testing the actions involving more *DoF*; extending the limb motion from planar to three-dimensional with hands orientation changes as well,
- analyzing stability of the human/exoskeleton behavior for avoiding unexpected motions and stresses.

References

1. Kazerooni, H. & Steger, R. The berkeley lower extremity exoskeleton. *Trans. ASME J. Dyn. Syst. Meas. Control.* **128**, 14–25 (2006).
2. Langane, S., Aoustin, Y., Arakalian & Chablat, D. *Investigation of the stresses exerted by an exosuit of a human arm* (Advanced technologies in robotics and intelligent systems, Springer, Cham, 425-435, 2020).
3. Siddique, N. *et al.* Prototype development of an assistive lower limb exoskeleton. In *2019 Int. Conf. on Robotics and Automation in Industry (ICRAI)*, 1–6, DOI: 10.1109/ICRAI47710.2019.8967351 (2019).
4. Grazi, L. *et al.* Design and experimental evaluation of a semi-passive upper-limb exoskeleton for workers with motorized tuning of assistance. *IEEE Trans. on Neural Syst. Rehabil. Eng.* **28**, 2276–2285, DOI: 10.1109/TNSRE.2020.3014408 (2020).
5. Popov, D., Gaponov, I. & Ryu, J.-H. Portable exoskeleton glove with soft structure for hand assistance in activities of daily living. *IEEE/ASME Trans. on Mechatronics* **22**, 865–875, DOI: 10.1109/TMECH.2016.2641932 (2017).
6. Kim, T., Jeong, M. & Kong, K. Bio-inspired knee joint of a lower-limb exoskeleton for misalignment reduction. *IEEE/ASME Trans. on Mechatronics* 1–1, DOI: 10.1109/TMECH.2021.3099815 (2021).
7. Sawicki, G. S. & Khan, N. S. A simple model to estimate plantarflexor muscle–tendon mechanics and energetics during walking with elastic ankle exoskeletons. *IEEE Trans. on Biomed. Eng.* **63**, 914–923, DOI: 10.1109/TBME.2015.2491224 (2016).
8. Meijneke, C. *et al.* Symbitron exoskeleton: Design, control, and evaluation of a modular exoskeleton for incomplete and complete spinal cord injured individuals. *IEEE Trans. on Neural Syst. Rehabil. Eng.* **29**, 330–339, DOI: 10.1109/TNSRE.2021.3049960 (2021).

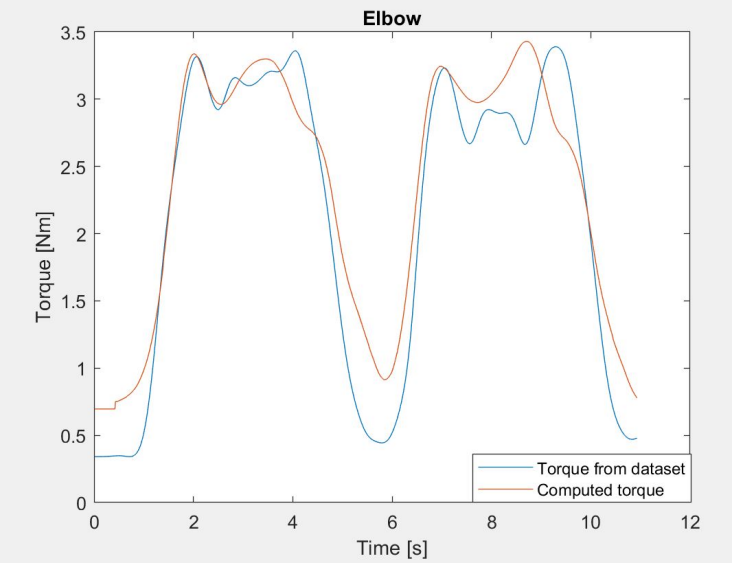

Figure 16. Elbow: comparison of the computed torques and the torques provided by the dataset.

9. Zhuang, Y. *et al.* Voluntary control of an ankle joint exoskeleton by able-bodied individuals and stroke survivors using emg-based admittance control scheme. *IEEE Trans. on Biomed. Eng.* **68**, 695–705, DOI: 10.1109/TBME.2020.3012296 (2021).

10. van Dijsseldonk, R. B., van Nes, I. J. W., Geurts, A. C. H. & Keijsers, N. L. W. Exoskeleton home and community use in people with complete spinal cord injury. *Sci. Reports* **10**, 15600, DOI: 10.1038/s41598-020-72397-6 (2020).

11. Anam, K. & Al-Jumaily, A. A. Active exoskeleton control systems: State of the art. *Procedia Eng.* **41**, 988–994, DOI: https://doi.org/10.1016/j.proeng.2012.07.273 (2012). International Symposium on Robotics and Intelligent Sensors 2012 (IRIS 2012).

12. Al Rezage, G. & Tokhi, M. Fuzzy pid control of lower limb exoskeleton for elderly mobility. In *2016 IEEE Int. Conf. on Automation, Quality and Testing, Robotics (AQTR)*, 1–6, DOI: 10.1109/AQTR.2016.7501310 (2016).

13. Bortole, M. *et al.* The h2 robotic exoskeleton for gait rehabilitation after stroke: Early findings from a clinical study wearable robotics in clinical testing. *J. neuroengineering rehabilitation* **12**, 54, DOI: 10.1186/s12984-015-0048-y (2015).

14. Kazerooni, H., Steger, R. & Huang, L. Hybrid control of the berkeley lower extremity exoskeleton (bleex). *The Int. J. Robotics Res.* **25**, 561 – 573, DOI: 10.1098/rspb.1938.0050 (2006).

15. Cavallaro, E., Rosen, J., Perry, J. & Burns, S. Real-time myoprocessors for a neural controlled powered exoskeleton arm. *IEEE Trans. on Biomed. Eng.* **53**, 2387–2396, DOI: 10.1109/TBME.2006.880883 (2006).

16. Kiguchi, K. & Imada, Y. Emg-based control for lower-limb power-assist exoskeletons. In *2009 IEEE Workshop on Robotic Intelligence in Informationally Structured Space*, 19–24, DOI: 10.1109/RIISS.2009.4937901 (2009).

17. Lenzi, T., De Rossi, S. M. M., Vitiello, N. & Carrozza, M. C. Proportional emg control for upper-limb powered exoskeletons. 628–631, DOI: 10.1109/IEMBS.2011.6090139 (2011).

18. Kenhub website, (accessed in august 2021).

19. Appell, P. *Dynamique des Systèmes - Mécanique Analytique* (Paris, P. Gauthiers-Villars, 1931).

20. Teachmeanatomy website - shoulder joint, (accessed in august 2021).

21. Teachmeanatomy website - elbow joint, (accessed in august 2021).

22. Too, J., Rahim, A. & Mohd, N. Classification of hand movements based on discrete wavelet transform and enhanced feature extraction. *Int. J. Adv. Comput. Sci. Appl.* **10**, DOI: 10.14569/ijacsa.2019.0100612 (2019).

23. Phinyomark, A., Phukpattaranont, P. & Limsakul, C. Fractal analysis features for weak and single-channel upper-limb emg signals. *Expert. Syst. with Appl.* **39**, 11156–11163, DOI: https://doi.org/10.1016/j.eswa.2012.03.039 (2012).

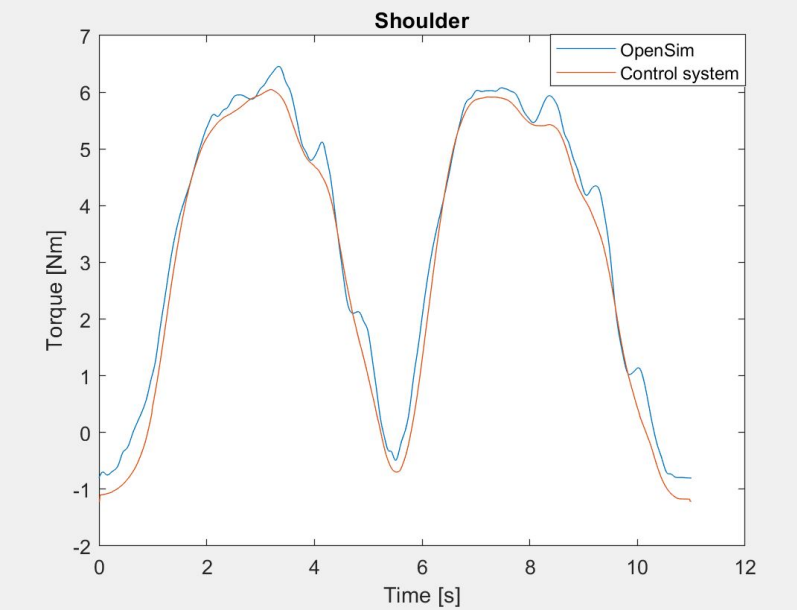

Figure 17. Shoulder: Comparison the torque obtained by *OpenSim* software and the torque delivered by the control system.

24. Chai, Y., Jia, L. & Zhang, Z. Mamdani model based adaptive neural fuzzy inference system and its application in traffic level of service evaluation. In *2009 Sixth International Conference on Fuzzy Systems and Knowledge Discovery*, vol. 4, 555–559, DOI: 10.1109/FSKD.2009.76 (2009).

25. Mamdani, J. H. & Assilian, S. An experiment in liguistic synthesis with a fuzzy logic controller. *Int. J. Man-Machine Stud.* **7**, 1–13 (1975).

26. Bland, J. M. & Altman, D. G. Statistical methods for assessing agreement between two methods of clinical measurement. *The lancet, Elsevier* **327**, 307–310 (1986).

27. Seth, A. *et al.* Opensim: Simulating musculoskeletal dynamics and neuromuscular control to study human and animal movement. *PLOS Comput. Biol.* **14**, e1006223, DOI: 10.1371/journal.pcbi.1006223 (2018).

Acknowledgments

We would like to express our gratitude to the Cluster Frame (https://next-isite.fr/frame) for supporting the project and to Professor Malgorzata Syczewska and the Kinesiology Laboratory, Department of Rehabilitation of The Children's Memorial Health Institute in Warsaw for sharing the motion recording infrastructure and professional support offered during data collecting. The collected data were made available by Warsaw University of Technology, Faculty of Power and Aeronautical Engineering - Dr.Marek Surowiec.

Author contributions statement

B.L. was involved in the numerical tests and the redaction of the article, Y.A. was the co-supervisor of B.L. and involved in numerical tests and in the redaction of the article, T.Z. was the co-supervisor of B.L., in the redaction of the article and defined the experimental protocol to get the experimental data.

Data availability

All data associated with this study are presented in the paper.

Competing interests

The authors declare no competing interests.

Additional information

Correspondence and requests for materials should be addressed to Y.A.

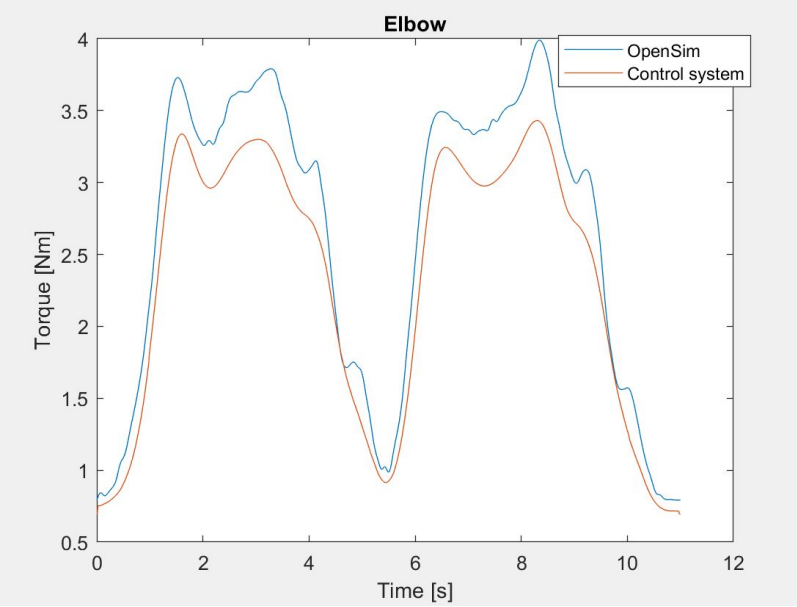

Figure 18. Shoulder: Comparison of torque obtained by the *OpenSim* and the torque delivered by the control system.